Electrochemical, FTIR, and UV/VIS Spectroscopic Properties of the ba_3 Oxidase from *Thermus thermophilus*†

Petra Hellwig,‡ Tewfik Soulimane,§ Gerhard Buse,§ and Werner Mäntele*,‡

Institut für Biophysik, Johann-Wolfgang-Goethe-Universität, Theodor-Stern-Kai 7 Haus 74, 60590 Frankfurt/M., Germany, and Institut für Biochemie, Rheinisch-Westfälischen-Technischen Hochschule, Klinikum Aachen, Paulwelstrasse 30, 52057 Aachen, Germany

Received February 11, 1999; Revised Manuscript Received April 19, 1999

ABSTRACT: The ba_3 cytochrome *c* oxidase from *Thermus thermophilus* has been studied with a combined electrochemical, UV/VIS, and FTIR spectroscopic approach. Oxidative electrochemical redox titrations yielded midpoint potentials of $E_{m_1} = -0.02 \pm 0.01$ V and $E_{m_2} = 0.16 \pm 0.04$ V for heme *b* and $E_{m_1} = 0.13 \pm 0.04$ V and $E_{m_2} = 0.22 \pm 0.03$ V for heme a_3 (vs Ag/AgCl/3 M KCl). Fully reversible electrochemically induced UV/VIS and FTIR difference spectra were obtained for the full potential step from −0.5 to 0.5 V as well as for the critical potential steps from −0.5 to 0.1 V (heme *b* is fully oxidized and heme a_3 remains essentially reduced) and from 0.1 to 0.5 V (heme *b* remains oxidized and heme a_3 becomes oxidized). The difference spectra thus allow to us distinguish modes coupled to heme *b* and heme a_3. Analogous difference spectra were obtained for the enzyme in D_2O buffer for additional assignments. The FTIR difference spectra reveal the reorganization of the polypeptide backbone, perturbations of single amino acids and of hemes *b* and a_3 upon electron transfer to/from the four redox-active centers heme *b* and a_3, as well as Cu_B and Cu_A. Proton transfer coupled to redox transitions can be expected to manifest in the spectra. Tentative assignments of heme vibrational modes, of individual amino acids, and of secondary structure elements are presented. Aspects of the uncommon electrochemical and spectroscopic properties of the ba_3 oxidase from *T. thermophilus* are discussed.

Cytochrome *c* oxidase (EC 1.9.3.1) is the terminal enzyme of the respiratory chain in mitochondria and many prokaryotes. As integral membrane protein, it catalyzes the reduction of dioxygen to water using electrons from cytochrome *c* according to the equation:

$$4\text{Cyt-}c\text{Fe}^{2+} + (4+n)\text{H}_i^+ + \text{O}_2 \rightarrow 4\text{Cyt-}c\text{Fe}^{3+} + n\text{H}_o^+ + 2\text{H}_2\text{O}$$

where H_i^+ and H_o^+ represent protons at the inner/outer side of the membrane. Four redox-active sites are involved in the electron transfer. Electrons from cytochrome *c* are first transferred to a homobinuclear copper A site (Cu_A) and then subsequently to heme *a*, and to heme a_3, which is located close to copper B (Cu_B), forming a heterobinuclear metal center where oxygen is reduced to water. The protons needed for water formation are taken up from the cytosolic side. The proton consumption and the coupled translocation of nH^+/e^- across the membrane contribute to the proton gradient needed to synthesize ATP (for reviews, see refs *1* and *2*).

Recently the crystal structures of cytochrome *c* oxidase from *P. denitrificans* (*3*, *4*) and from bovine heart (*5*, *6*) have been solved. Two putative proton pathways, called "K-pathway and D-pathway", according to specific lysine "Lys-354" and aspartic acid "Asp-124" residues involved, have been identified (the amino acid numbering in this paper refers to that of subunit I of the aa_3 oxidase from *P. denitrificans* if not specifically mentioned). A third proton pathway has been recently proposed by Yoshikawa et al. (*7*). The crucial residue Asp-51 (numbering for bovine enzyme) suggested to be involved in the H-pathway is not conserved in the plant and bacterial oxidases (*7*). The K-pathway leads from the cytoplasm to the binuclear center through Ser-191, Lys-354, Thr-351, and Tyr-280. Interestingly, the latter has been suggested to be covalently linked to one of the Cu_B ligands (His-276) (*4*, *7*). This suggestion has been verified using protein chemical methods (*8*). Mutation of Lys-354 inactivates the oxidase, and heme a_3 is difficult to reduce (*9*−*11*). Mutation of Thr-351 decreases the activity of the enzyme. These results suggest that the K-pathway is used for proton uptake coupled to the reduction of the heme a_3 Cu_B site. It is the turnover with O_2 that is inhibited in the Lys-354 mutants, whereas the enzyme is still active with H_2O_2 as electron acceptor (*12*, *13*), suggesting that the protons involved in proton pumping follow a different path. The D-pathway leads from Asp-124 via six polar residues to a highly conserved glutamic acid residue, Glu-278. In flow-flash experiments with Asp-124 and Glu-278 mutants, the reoxidation of the enzyme stopped at the peroxy (P) intermediate, with Cu_A remaining reduced (*14*). It was also found that proton pumping in the ferryl intermediate →

† Financial support from DFG to W.M. and G.B. (BU463/3-2) is gratefully acknowledged.

* To whom correspondence should be addressed. Email: maentele@biophysik.uni-frankfurt.de. Telephone: 49-69-6301-5835. Fax: 49-69-6301-5838.

‡ Johann-Wolfgang-Goethe-Universität.

§ Klinikum Aachen.

10.1021/bi9903401 CCC: $18.00
Published on Web 07/08/1999

oxidized state (F → O) transition was impaired in the Glu-278 mutant (*15*). These results indicate that Asp-124 and Glu-278 are relevant for oxygen reduction and proton transfer (*1, 2*).

The thermophilic Gram-negative eubacterium *Thermus thermophilus* HB8 (ATCC 27634) expresses two different terminal oxidases. Concerning the hemes incorporated, they belong to the caa_3 and ba_3 types (*16, 17*), however, with a geranyl/geranyl side chain at heme *a* (*18*). The ba_3 oxidase is the smallest known cytochrome *c* oxidase. It consists of only two subunits (*19*) which are distantly related to subunits I and II of common cytochrome *c* oxidases (*20*). It was shown that the ba_3 oxidase reacts with cytochrome c_{552} that appears to be the physiological substrate (*21, 22*). The high interest in the aberrant ba_3 oxidase is based on: (i) the amino acid sequence reveals a very low homology with most terminal oxidases (*23*) and belongs to the Sox-B cluster (*24*), (ii) all crucial amino acids in the D- and K-pathways discussed for water formation and proton translocation are not conserved in the ba_3 oxidase, (iii) several studies using EPR, FTIR, resonance Raman, and magnetic CD spectroscopy clearly showed that the heme a_3-Cu_B center of the ba_3 oxidase has peculiar ligand binding properties (*21, 22, 25*−*28*), and (iv) its crystal structure is being solved (*29*). Nevertheless, the enzyme is an electrogenic proton pump that couples oxygen reduction to the consumption of 1 H^+/e^- and the translocation of 0.4−0.5 H^+/e^- across the membrane (*30*).

FTIR difference spectroscopy is a sensitive method to detect the structural changes upon electron transfer and coupled proton transfer. Although changes of vibrational modes may be observed throughout the full mid-infrared, focus is on the modes of diagnostic relevance which are observable between 2200 and 1200 cm^{-1}. This spectral range was presented for the difference spectra of the light induced CO photolysis from bovine heart oxidase (*31*) and bo_3 oxidase from *E. coli* (*32*). FTIR difference spectra induced by photoreduction have been presented in ref *33*. The combination of protein electrochemistry and FTIR difference spectroscopy has been demonstrated by studies on aa_3 oxidase from *Paracoccus denitrificans* (*34*−*36*). In this paper we present an analysis of the electrochemical, UV/VIS, and FTIR spectroscopic properties of the ba_3 oxidase from *Thermus thermophilus*.

MATERIALS AND METHODS

Sample Preparation. For the expression of the ba_3 oxidase, *Thermus thermophilus* HB8 cells were grown at 70 °C in 100 L of culture medium using a stainless-steel jar fermenter under restricted aeration. The ba_3-type cytochrome *c* oxidase was prepared according to a new protocol: 100 g of frozen cells was thawed in 500 mL of 100 mM Tris/HCl, pH 7.6, containing 200 mM KCl and 800 mg of lysozyme. After a 60 min stirring period, the suspension was centrifuged. For the solubilization of the respiratory complexes, the pellet was resuspended in 500 mL of 100 mM Tris/HCl, pH 7.6, adjusted to 5% Triton X-100, stirred for 3 h, and centrifuged at 17700*g* (Beckman JA-10 rotor, 10 000 rpm) at 4 °C. The supernatant was diluted with 5 L of H_2O and chromatographed on a DEAE-Biogel Agarose column (BioRad) in 0.1% Triton X-100, 10 mM Tris/HCl, pH 7.6. Fractions containing the ba_3 oxidase were pooled, concentrated (Minitan 10 000; Millipore), and rechromatographed twice on Fractogel TMAE-650 (S) (MERCK); the detergent 0.1% Triton X-100 was changed to 0.05% dodecyl-β-D-maltoside. Fractions containing ba_3 oxidase were again collected, concentrated, and purified by gel filtration on Superdex 200 (Pharmacia) in 50 mM Tris/HCl, pH 7.6, containing 0.1% dodecyl-β-D-maltoside. The purified ba_3 oxidase was concentrated by Ultrafiltration (Centricon 100 000; Amicon), desalted by passing through a Sephadex G-25 column, shock frozen in liquid nitrogen, and stored at −74 °C.

For electrochemistry, the ba_3 oxidase was solubilized in *n*-decyl-β-D-maltopyranoside, 100 mM phosphate buffer (pH 7) containing 50 mM KCl and was concentrated to approximately 0.5 mM using Microcon ultrafiltration cells (Millipore). Exchange of H_2O against D_2O was performed by repeatedly concentrating the enzyme and rediluting it in a D_2O buffer. H/D exchange was found better than 80% as judged from the shift of the amide II mode at 1550 cm^{-1} in the FTIR absorbance spectra (data not shown).

Electrochemistry. The ultra-thin-layer spectroelectrochemical cell for UV/VIS and IR was used as previously described (*37, 38*). Sufficient transmission in the 1800−1000 cm^{-1} range, even in the region of strong water absorbance around 1645 cm^{-1}, was achieved with the cell path length set to 6−8 μm. The gold grid working electrode was chemically modified by a 2 mM pyridine-3-carboxyaldehyde thisemicarbazone (PATS-3) solution as reported before (*35*). To accelerate the redox reaction, 15 different mediators were added as reported in ref *35* (except $K_4[Fe(CN)_6]$) to a total concentration of 40 μM each. At this concentration, and with the path length below 10 μm, no spectral contributions from the mediators in the VIS and IR range could be detected in control experiments with samples lacking the protein, except for the PO modes of the phosphate buffer between 1200 and 1000 cm^{-1}. As a supporting electrolyte, 50 mM KCl was added. Approximately 5−6 μL of the protein solution was sufficient to fill the spectroelectrochemical cell. Potentials quoted with the data refer to the Ag/AgCl/3 M KCl reference electrode; add +208 mV for SHE′ (pH 7) potentials.

Spectroscopy. FTIR and UV/VIS difference spectra as a function of the applied potential were obtained simultaneously from the same sample with a setup combining an IR beam from the interferometer (modified IFS 25, Bruker, Germany) for the 4000−1000 cm^{-1} range and a dispersive spectrometer for the 400−900 nm range as reported previously (*38, 39*). First, the protein was equilibrated with an initial potential at the electrode, and single-beam spectra in the VIS and IR range were recorded. A potential step toward the final potential was then applied, and single-beam spectra of this state were again recorded after equilibration. Difference spectra as presented here were then calculated from the two single-beam spectra with the initial single-beam spectrum taken as reference. No smoothing or deconvolution procedures were applied. The equilibration process for each applied potential was followed by monitoring the electrode current and by successively recording spectra in the visible range until no further changes were observed. The equilibration generally took less than 8 min under the conditions (protein concentration, electrode modification, mediators) for the potential steps reported. Typically, 128 interferograms at 4 cm^{-1} resolution were coadded for each single-beam IR

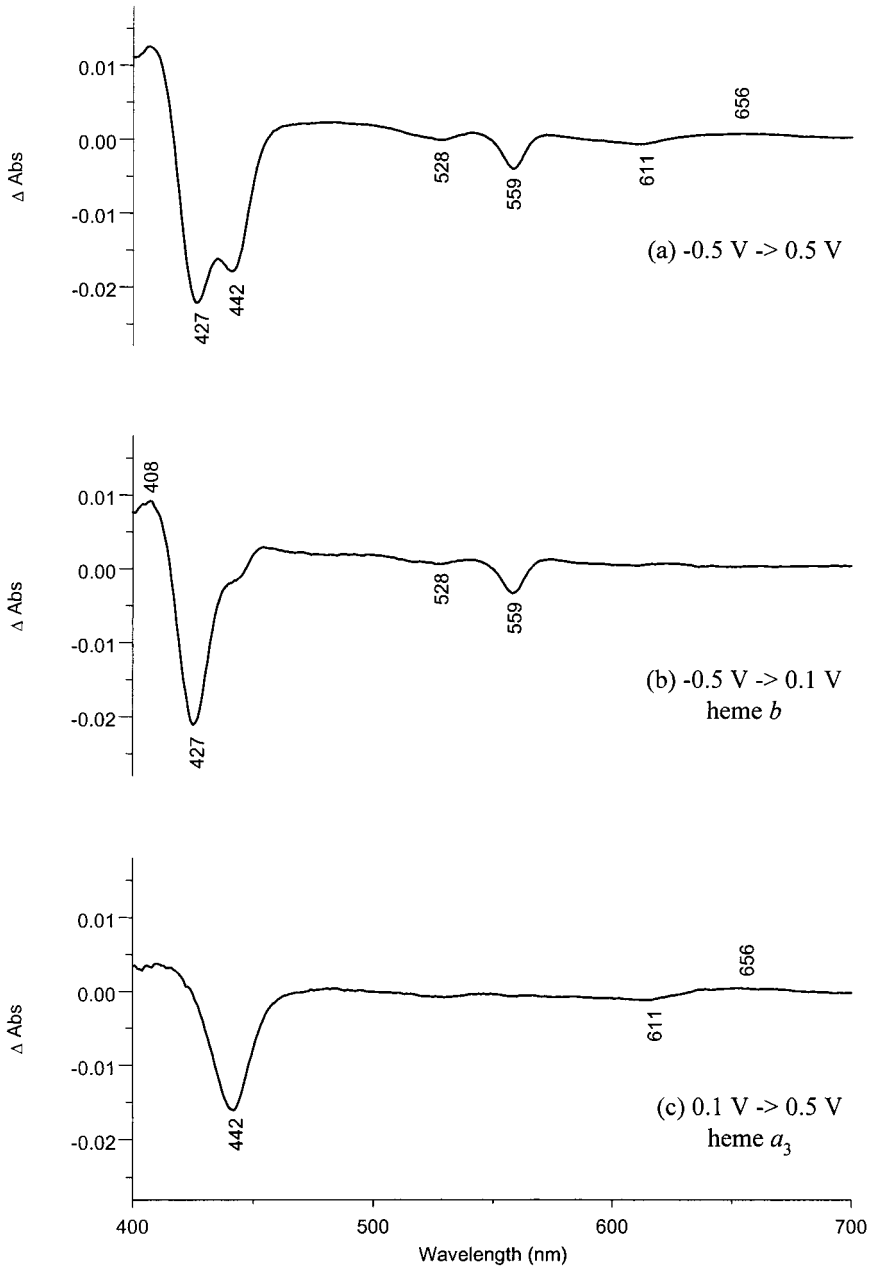

FIGURE 1: Oxidized-minus-reduced UV/VIS difference spectra of the ba_3 oxidase from *T. thermophilus* obtained for a potential step from −0.5 to 0.5 V (a) and for the selected potential steps from −0.5 to 0.1 V where the heme *b* contributions dominate (b) and from 0.1 to 0.5 V (c) where the heme a_3 contributions dominate. All potentials are quoted vs Ag/AgCl/3 M KCl. For experimental conditions, see Materials and Methods.

spectrum and Fourier-transformed using triangular apodization. Differences in sample concentration and path length were taken into account by normalizing the FTIR difference spectra on the difference signal of the sample in the UV/VIS at 559 nm.

Redox Titrations. The redox-dependent absorbance changes of the cytochrome *c* oxidase from *T. thermophilus* were studied by performing electrochemical redox titrations in the UV/VIS spectral range. The redox titrations were performed by stepwise setting the potential and recording the spectrum after sufficient equilibration. Typically, data were recorded at steps of 55 mV. All measurements were performed at 5 °C. The midpoint potentials, E_m, and the number *n* of transferred electrons were obtained by adjusting a calculated Nernst curve to the measured absorbance change at a single wavelength by an interactive fit. All parameters have to be adjusted manually until the theoretical Nernst curve and the measured data matched well (*fit by eye*).

RESULTS AND DISCUSSION

Electrochemically Induced UV/VIS Difference Spectra. Figure 1 a shows the oxidized-minus-reduced UV/VIS difference spectra of the ba_3 oxidase from *T. thermophilus* obtained for a potential step from −0.5 to 0.5 V (vs Ag/AgCl/3 M KCl). In the oxidized-minus-reduced spectra, the positive signals correlate with the oxidized and the negative signals with the reduced form of the enzyme. The difference spectra are exact mirror images to the reduced-minus-oxidized spectra (data not shown), indicating the full reversibility of the electrochemical reaction. For the reduced form, the Soret band can be observed at 427 and 441 nm; for the oxidized form at 408 nm. The β-band can be seen at

528 nm, the α-band at 559 and 611 nm. A broad signal at 656 nm can be observed for the oxidized form.

The difference signals observed in the visible spectral range from 400 to 700 nm can be assigned to contributions of hemes *b* and a_3 (*40*, *41*), whereas Cu_B does not show detectable absorptions in the visible spectral range (*42*). The bands observed at 427, 528, and 559 nm are characteristic for low-spin hemes *b*. The difference signals at 441 and at 611 nm can be assigned to high-spin heme a_3 (*42*). At 656 nm, a band can be seen which has been previously assigned to the high-spin heme a_3 in bovine heart oxidase (*43*). In addition to the heme contributions, weaker signals from the Cu_A center can be expected at approximately 480, 530, and 834 nm, based on investigations on the isolated subunit II fragment of aa_3 oxidase (*44*, *45*). However, these signals are superimposed by the intense contributions from the hemes.

In a recent publication (*7*), the presence of a peroxy ligand in the binuclear center of the cytochrome *c* oxidase from bovine heart was postulated for the oxidized state. We found no evidence here for the expected shift of the α-band described for the development of the peroxy form in refs *40* and *41*. However, this was not explicitly investigated for the ba_3 oxidase from *T. thermophilus* yet. In addition, a short lifetime was reported for the peroxy state.

Figure 1 shows the oxidized-minus-reduced UV/VIS difference spectra of the ba_3 oxidase obtained for a potential step from −0.5 to 0.5 V (Figure 1a) and for the critical potential steps from −0.5 to 0.1 V (Figure 1b) and from 0.1 to 0.5 V (Figure 1c). In the UV/VIS difference spectra obtained for the critical potential step from −0.5 to 0.1 V, the fully developed Soret (427 nm), β-band (528 nm), and α-band (559 nm) of heme *b* can be seen. The characteristic absorptions of heme a_3 only contribute approximately 20% of the amplitudes in this potential range (cf. titration curves in Figure 2). For the potential step from 0.1 to 0.5 V, the contribution of heme a_3 develops. Clear arguments for our assignment are the characteristic optical properties of the two heme centers, differing due to their coordination and spin state and clearly distinguishable in the titration presented here. The potential-dependent absorbance changes observed in the higher potential range (Figure 1c) show characteristic features (peak position and intensity) of high-spin 5-coordinated heme a_3 model compounds described by (*42*). The changes observed for the lower potential range (Figure 1b) can be clearly attributed to heme *b*. The possibility of separating the heme contributions as documented unequivocally by separated UV/VIS spectra will be accordingly used for the IR spectroscopy in order to support attribution of heme modes to heme *b* or a_3.

UV/VIS Redox Titrations. Figure 2 shows a redox titration of the ba_3 oxidase in the potential range from −0.5 to +0.5 V in the visible spectral range. The potential-dependent development of the α-band at 559 nm is shown in Figure 2a. The closed circles represent the measured data interactively fitted to a calculated Nernst curve (cf. Materials and Methods). Two redox midpoint potentials can be determined from this fit: $E_{m_1} = -0.02 \pm 0.01$ V and $E_{m_2} = 0.16 \pm 0.04$ V. The error was estimated from the standard deviation of several titrations. We assign these midpoint potentials to heme *b* which contributes at 559 nm, as discussed above. The potential-dependent development of the Soret band of

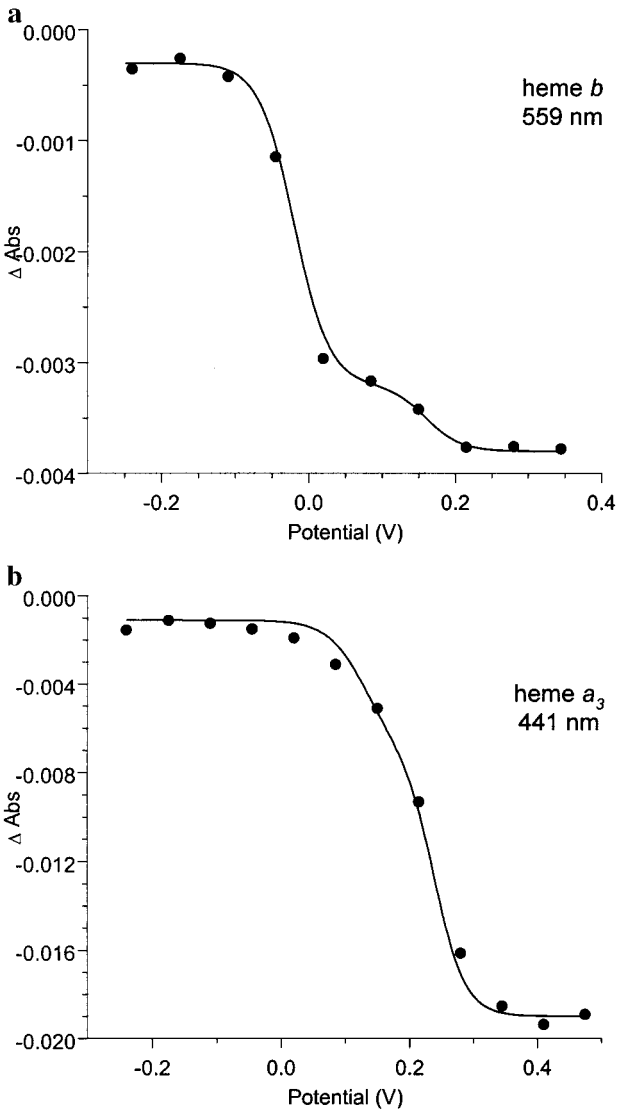

FIGURE 2: Potential dependence of the α-band of heme *b* at 559 nm (a) and of the Soret band of heme a_3 at 441 nm (b). Closed circles represent the oxidative redox titration. The data were interactively fitted to a calculated Nernst curve (solid line). Two midpoint potentials can be determined for each heme from these fits: $E_{m_1} = -0.02 \pm 0.01$ V and $E_{m_2} = 0.16 \pm 0.04$ V for heme *b*, and $E_{m_1} = 0.13 \pm 0.04$ V and $E_{m_2} = 0.22 \pm 0.03$ V for heme a_3.

heme a_3 at 441 nm (Figure 2b) reveals two midpoint potentials at $E_{m_1} = 0.13 \pm 0.04$ V and $E_{m_2} = 0.22 \pm 0.03$ V. These potentials can be assigned to heme a_3. A clear argument for the attribution of the potentials to heme *b* or a_3 is the optical properties of each heme described above.

The potentials of the hemes and especially the order in which the redox transitions can be observed are uncommon as compared to bovine heart oxidase (*46*−*51*). For the bovine heart enzyme, undistinguishable midpoint potentials of the two heme centers in the absence of inhibitors are reported due to their cooperativity and to the cooperativity with Cu_B (*46*−*51*). For the interpretation of the complex data describing the cooperative interactions between the redox centers, several models have been developed. The most prominent one is the *neoclassical model* (*46*). In the bovine heart aa_3 oxidase, a triphasic titration curve describing the cooperative interactions, with both hemes contributing through the phases, is expected. Cu_B cooperativity with the hemes causes this complex picture (*46*, *47*). The potential-dependent

development of the contributions in the UV/VIS is first dominated by heme a_3 and then by the heme *a* contributions.

In the oxidative titrations presented here, first contributions from heme *b* and then from heme a_3 can be seen, describing a biphasic development for each of the hemes. The potential-dependent developments of the heme redox states clearly differ from those reported for bovine heart oxidase. The two steps in the titration curve of each heme might be explained in the sense of the *neoclassical model* with the steps describing the heme coupled to the different cofactors. If we assume that both hemes contribute at the same absorption (as in the bovine heart oxidase), a triphasic curve as described for bovine heart can be found, however, with inverted potentials for hemes *b* and a_3. The contribution of heme *b* could be determined to amount to approximately 80% in the UV/VIS difference spectra for a potential step from −0.5 to 0.1 V. However, the functional role of the deviations cannot be explained yet. We keep in mind that *T. thermophilus* is an organism living at extreme environmental conditions, at approximately 80 °C. The measurements presented here have been performed at 5 °C, and the effect of higher temperature on the potentials should be regarded. However, potential titrations of the caa_3 oxidase from *T. thermophilus* at 5 °C showed titration curves for hemes *a* and a_3 describing the same triphasic shape and potentials close to those of bovine heart oxidase (P. Hellwig, unpublished results). On the basis of the determined potentials, we assume that electron-transfer measurements could reveal uncommon rates as compared to bovine heart oxidase. In a recent publication, the unique kinetic behavior of the ba_3 oxidase from *T. thermophilus* in the reaction with oxygen and cyt *c*552 as well as ligand binding dynamics are reported (*21*). On that basis, uncommon electrochemical properties of the hemes and Cu_B are to be expected (*21*).

Electrochemically Induced FTIR Difference Spectra in H_2O and D_2O. Figure 3a−c shows the oxidized-minus-reduced FTIR difference spectra of the ba_3 oxidase for the full potential step from −0.5 to 0.5 V (Figure 3a) and for partial potential steps from −0.5 to 0.1 V (Figure 3b) and from 0.1 to 0.5 V (Figure 3c), respectively. Figure 4a−c shows the oxidized-minus-reduced FTIR difference spectrum of the cytochrome *c* oxidase equilibrated in D_2O buffer obtained for the same potential steps as in Figure 3. The difference spectra obtained for D_2O buffer (Figure 4a−c) show spectral features comparable to those in H_2O (Figure 3a−c). The major signals are almost unaffected by deuteration; however, variations in band amplitudes can be observed in particular between 1700 and 1646 cm^{-1} and will be discussed in the following paragraphs.

The entity of difference signals represents the total of molecular changes concomitant with the redox reactions, i.e., conformational changes or charge redistributions in the cofactor sites, and thus describes the scenario of the enzyme's function. In the FTIR difference spectra, signals reflecting the reorganization of the hemes, of the polypeptide backbone and amino acid side chains occurring upon electron transfer of the four redox-active centers (hemes b/a_3, Cu_A, and Cu_B), can be expected. In addition, proton transfer coupled to the redox process can be expected to manifest in the spectra.

In the following paragraphs, the difference spectra will be described and discussed. Tentative assignments will be presented on the basis of comparison to IR and Raman spectra of heme model compounds and other oxidases, FTIR spectra of isolated amino acids and small peptides as model compounds, and information on contributions from the secondary structure from infrared absorbance spectra and the deconvolution of the amide I region.

Buffer Contributions. In the lower spectral region from 1200 to 1000 cm^{-1}, a broad difference structure with a maximum at 1160 cm^{-1} and a minimum at 1088 cm^{-1} upon oxidation can be observed (Figure 3a). Upon H/D exchange, an upshift of the signals to 1182 and 1098 cm^{-1} can be observed (Figure 4a). This indicates a change in the hydrogen bonding strength to/from the contributing group after H/D exchange. As previously described for the cytochrome *c* oxidase from *P. denitrificans*, these bands can be assigned to PO modes caused by deprotonation of the phosphate buffer, correlating with proton uptake by the protein and the mediators upon electron transfer (*34*). If other buffers are used, these PO signals are absent, and modes characteristic for the buffers used appear. It was shown recently that the ba_3 oxidase from *T. thermophilus* acts as a proton pump (*30*). It is thus conceivable that the signals at 1160 and 1088 cm^{-1} reflect proton uptake coupled to proton transfer in the protein. We keep in mind that proton uptake from the redox reactions of the mediators contributes here as well. Blank difference spectra of samples lacking the protein verify that the proton uptake/release of the mediators can be observed in the buffer modes; however, no infrared signals from the mediators can be seen (data not shown).

Assignment of Heme Modes. In the approach presented here, the contributions of both hemes can be distinguished on the basis of the electrochemically induced FTIR difference spectra for the potential step from −0.5 to 0.1 V (Figure 3/4b) and 0.1 and 0.5 V (Figure 3/4c), as discussed for the UV/VIS difference spectra, and tentative assignments of characteristic heme vibrational modes and comparison to resonance Raman data for the same enzyme are possible (*27, 42, 52, 53*). The nomenclature used in this paper to describe heme modes was described in Spiro and Li (*54*) and was previously introduced in ref *55*. For the electrochemically induced FTIR difference spectra, C−C and C−N modes of the porphyrin ring, C═O modes of protonated or deprotonated propionates, and C═C vibrations of the vinyl substituents can be expected originating from hemes *b* and a_3. In addition, C═O vibrations of the heme a_3 formyl group can be found.

(A) Porphyrin Ring Modes. Model compound investigations indicate that the C*a*C*m* vibration (ν_{37}) from the porphyrin ring can be expected between 1586 and 1655 cm^{-1} (*56*). In resonance Raman spectra of the oxidized caa_3 oxidase from *T. thermophilus*, a signal at 1584 cm^{-1} was assigned to the ν_{37} vibration of heme a_3 (*53*). Park et al. (*31*) have assigned signals at 1565 and 1580 cm^{-1} to the ν_{37} vibration in photochemically induced FTIR difference spectra of CO-poisoned beef heart oxidase. A direct comparison to these difference spectra obtained by completely different techniques, and of native and poisoned enzyme, however, must be handled cautiously. In the electrochemically induced FTIR difference spectra of the cytochrome *c* oxidase from *P. denitrificans*, a signal at 1588 cm^{-1} was assigned to the ν_{37} vibration of heme a_3 (*55*). In the spectral region where the ν_{37} vibration is expected (1586 and 1655 cm^{-1}), several overlapping signals can be observed (Figure 3/4c). The difference signal at 1610 cm^{-1} is a possible candidate for

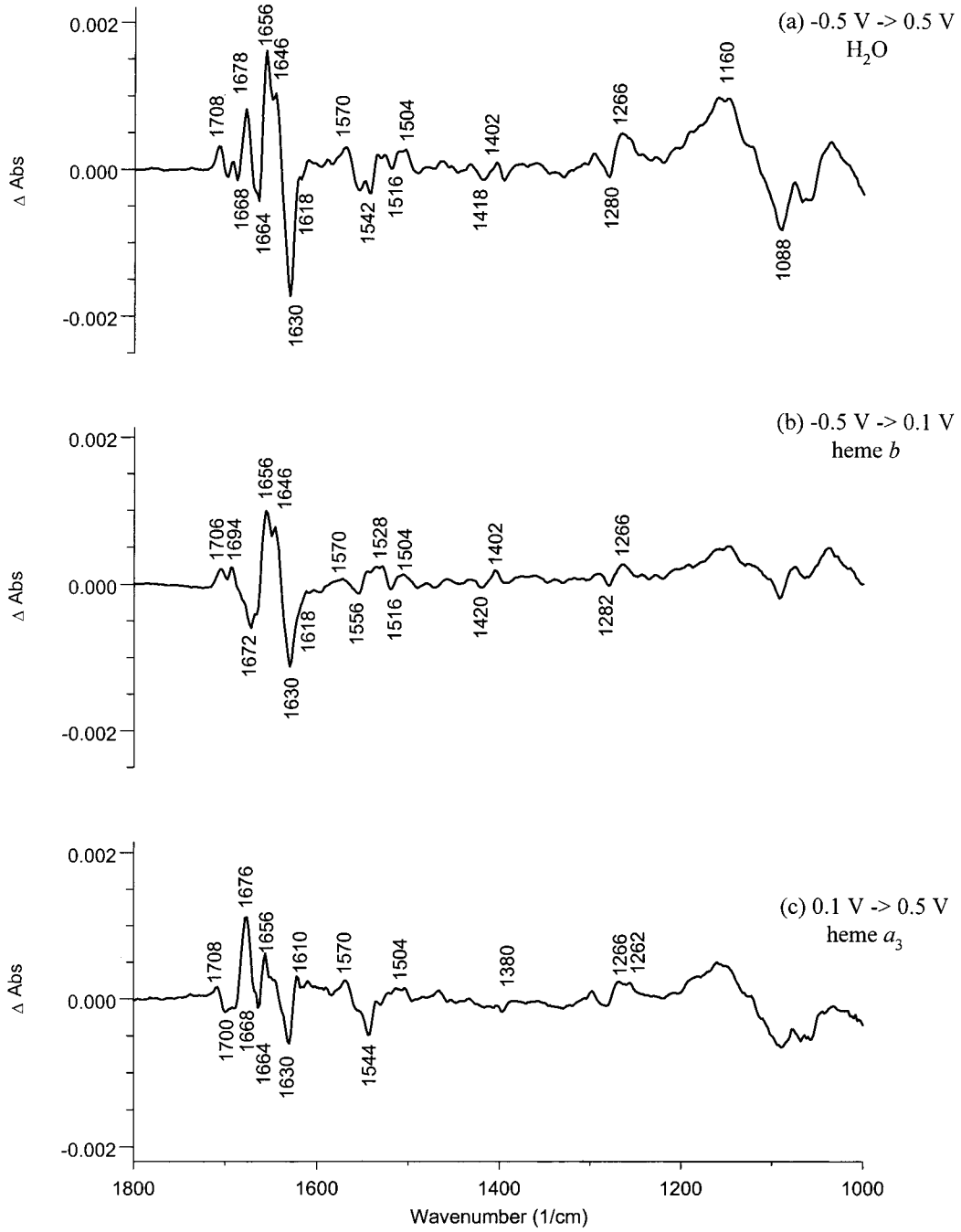

FIGURE 3: Oxidized-minus-reduced FTIR difference spectra of the *ba*$_3$ oxidase from *T. thermophilus* equilibrated in H_2O buffer (a) and for the selected potential steps from −0.5 to 0.1 V where the heme *b* contributions dominate (b) and from 0.1 to 0.5 V (c) where the heme a_3 contributions dominate.

the ν_{37} vibration of heme a_3. In electrochemically induced FTIR difference spectra of heme *b* model compounds, the ν_{37} mode was assigned to signals at 1571 cm^{-1} (oxidized form) and 1553 cm^{-1} (reduced form) (*57*). On the basis of these model compound spectra, we propose the involvement of the ν_{37} vibrational mode of heme *b* in the difference signals at 1570/1574 and 1556/1554 cm^{-1} observed in Figures 3 and 4b.

The C*b*C*b* vibration (ν_{38}) was observed between 1529 and 1535 cm^{-1} in heme *b* model compound studies (*57*). In the electrochemically induced FTIR difference spectra in Figure 3/4, the ν_{38} vibrational mode cannot be identified. In spectra of type *a* porphyrins, the ν_{38} vibrational mode is expected to split due to the reduced symmetry of the porphyrin ring as compared to type *b* porphyrins (*42*, *52*). The *x* and *y* axes describing the orientation of the split vibration (ν_{38x} and ν_{38y}) have been introduced in ref *55*. In resonance Raman spectra of reduced *caa*$_3$ oxidase from *T. thermophilus* (*53*) and from *aa*$_3$ beef heart oxidase, the ν_{38y} vibrational mode of heme a_3 could be identified at 1531 cm^{-1} (*53*). In the electrochemically induced FTIR difference spectra of the cytochrome *c* oxidase from *P. denitrificans*, the ν_{38y} vibrational mode of heme a_3 could be identified at 1528 cm^{-1}. In the corresponding difference spectra presented here (Figures 3, 4c), no significant difference signal can be observed at this position. The strong negative signal at 1542 cm^{-1} is a possible candidate for the ν_{38y} vibrational mode. This would be an uncommon absorption as compared with the beef heart and

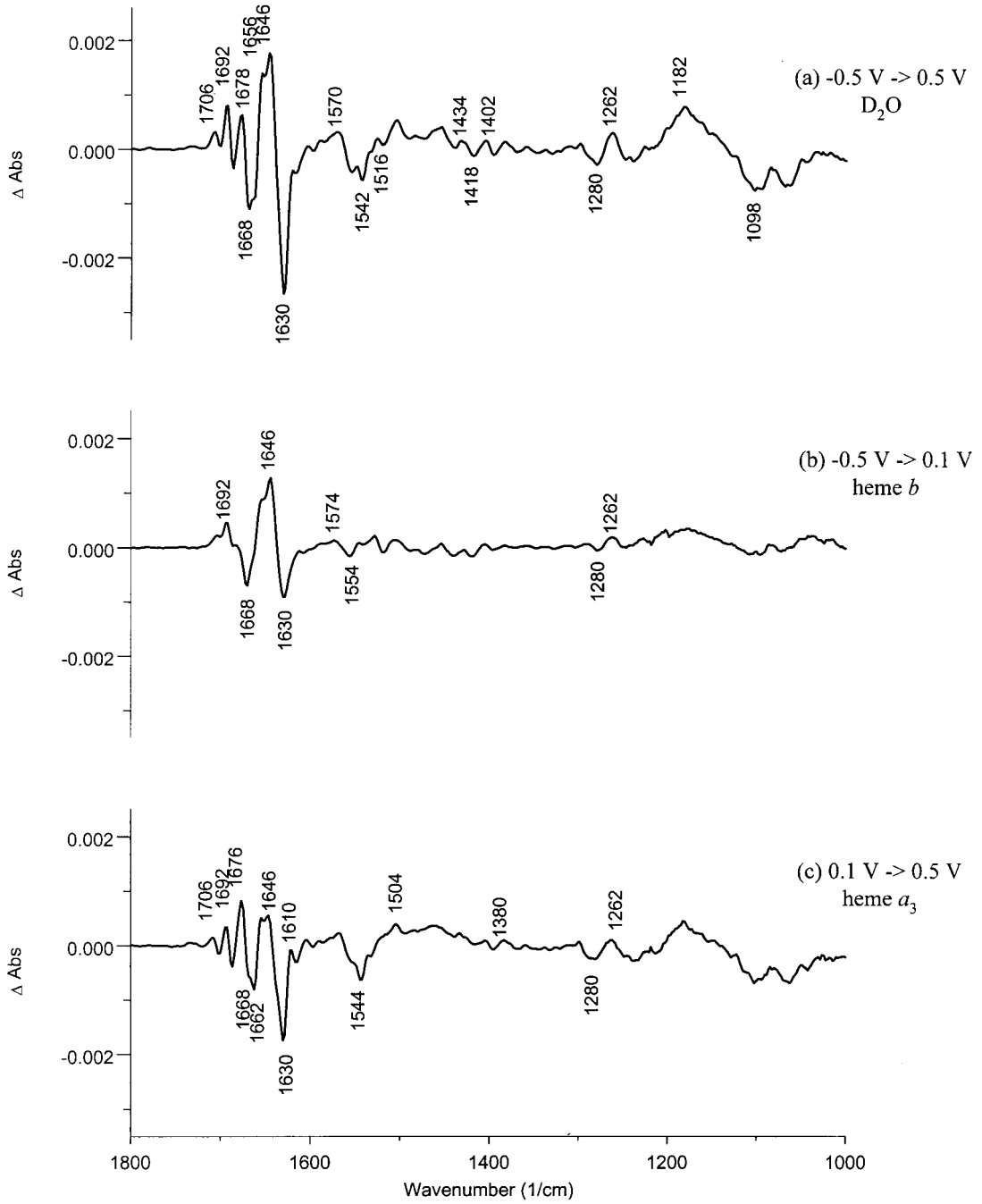

FIGURE 4: Oxidized-minus-reduced FTIR difference spectra of the ba_3 oxidase from *T. thermophilus* equilibrated in D_2O buffer (a) and for the selected potential steps from −0.5 to 0.1 V where the heme *b* contributions dominate (b) and from 0.1 to 0.5 V (c) where the heme a_3 contributions dominate.

P. denitrificans oxidase and may indicate differences in the local site of the binuclear center. The ν_{38x} vibrational modes can be expected at 1565−1570 cm^{-1} (*56*) and could be observed for heme a_3 in the *P. denitrificans* oxidase at 1564 cm^{-1} (*55*). In the electrochemically induced FTIR difference spectra of ba_3 oxidase from *T. thermophilus* presented in Figures 3c and 4c, the involvement of that vibration in the 1570 cm^{-1} difference band is conceivable.

In the photochemically induced FTIR difference spectra of CO-poisoned beef heart oxidase, the ν_{38} vibrational mode was assigned to signals at 1565, 1540, and 1531 cm^{-1} (*31*); the splitting of the ν_{38} vibrational mode (discussed before), however, was not discussed. Oertling et al. (*27*) attribute in resonance Raman spectra of the ba_3 oxidase from *T. thermophilus* a signal at 1559 cm^{-1} (reduced form) to the ν_{38} vibrational mode; however, the splitting of the mode is not discussed there.

The absorption of the C*a*N vibration, termed ν_{41}, can be expected between 1319 and 1389 cm^{-1} and could be identified in resonance Raman spectra at 1374 cm^{-1} for the oxidized and at 1365 cm^{-1} for the reduced cytochrome *c* oxidase from *P. denitrificans* (*52*). Park et al. (*31*) proposed difference bands at 1371 and 1366 cm^{-1} for the ν_{41} vibrational modes from photochemically induced FTIR difference spectra of CO-poisoned beef heart oxidase. In the electrochemically induced FTIR difference spectra of the cytochrome *c* oxidase from *P. denitrificans*, a signal at 1362 cm^{-1} (reduced form) and a signal at 1380 cm^{-1} (oxidized

form) could be observed for heme a_3 (*55*). In Figures 3c and 4c, a difference signal at 1380 cm^{-1} can be tentatively assigned to the ν_{41} vibrational mode of the hemes. The C*m*H vibration (δ_{42}) was observed between 1150 and 1268 cm^{-1} in heme *b* model compound spectra (*57*). The positive signal at 1266 cm^{-1} can be tentatively assigned to the δ_{42} vibrational mode.

It is clear that, in addition to the modes assigned here, further C−C or C−N vibrations of the porphyrin ring (ν_4,ν_{39}) will contribute to the electrochemically induced FTIR difference spectra. However, we refrain from discussing and assigning these modes on the basis of the data presented here.

(B) Formyl Substituent Modes. The ν(C═O) mode of the formyl group of hemes can be expected between 1680 and 1606 cm^{-1}, depending on hydrogen bonding with neighboring amino acids. In resonance Raman spectra of the ba_3 oxidase from *T. thermophilus*, the ν(C═O) mode of the oxidized form of heme a_3 was observed at 1675 cm^{-1} (*58*)/ 1676 cm^{-1} (*27*) and for the reduced form at 1671 cm^{-1} (*58*)/ 1669 cm^{-1} (*27*). In the electrochemically induced FTIR difference spectra of the cytochrome *c* oxidase from *P. denitrificans*, the ν(C═O) CHO mode of the oxidized heme a_3 could be assigned to a signal at 1678 cm^{-1} and that of the reduced form to a signal at 1668 cm^{-1} (*55*). Resonance Raman data substantiate these assignments (*42*, *52*).

In the electrochemically induced FTIR difference spectra in Figure 4, difference signals can be observed at 1676 cm^{-1} (oxidized form) and 1668 cm^{-1} (reduced form). The difference spectra for the critical potential step from 0.1 to 0.5 V (Figure 3c), where mainly contributions from heme a_3 can be expected, reveal that the discussed bands correlate with the electron transfer to/from heme a_3, supporting an assignment of the signals to the ν(C═O) CHO mode of heme a_3.

As mentioned above, the absorption of the ν(C═O) CHO mode depends on hydrogen bonding with neighboring amino acids. The formyl substituent of heme a_3 in the cytochrome *c* oxidase from *P. denitrificans* as well as from bovine heart oxidase does not form a hydrogen bond, as proposed on the basis of the respective structures (*3*−*7*). Direct comparison of the absorption of the ν(C═O) CHO mode of heme a_3 in *P. denitrificans* and *T. thermophilus*, as well as of resonance Raman data, indicates that there is no hydrogen bonding from/to the formyl group in heme a_3 in *T. thermophilus* ba_3 oxidase. Similarities in the direct environment of this substituent can thus be expected, with only smaller deviations expected from the 5−6 cm^{-1} difference between the ν(C═O) CHO modes for the reduced form (see above).

(C) Vinyl Substituent. The $\nu(C_\alpha{=}C_\beta)$ vibration of the vinyl substituent was observed at 1620 cm^{-1} in heme *b* model coumpound investigations (*57*). In resonance Raman spectra, a difference signal at 1618 cm^{-1} was assigned to the $\nu(C_\alpha{=}C_\beta)$ vibrational mode of heme a_3 (*27*). The $\nu(C_\alpha{=}C_\beta)$ vibrational mode of heme *b* is probably contributing as a shoulder of the strong signal at 1630 cm^{-1}.

(D) Heme Propionate Modes. In the spectral region characteristic for the ν(C═O) mode of protonated carboxylic groups of the heme propionates, difference signals can be observed between approximately 1708 and 1678 cm^{-1} (Figure 3a). In the typical spectral range for the $\nu(COO^-)^{as}$ vibration between 1570 and 1530 cm^{-1}, some distinct difference signals can be observed (Figures 3 and 4). Similarly, signals at 1390 cm^{-1} are observed which could be characteristic for the $\nu(COO^-)^{s}$ vibration.

For the aa_3 cytochrome *c* oxidase from *P. denitrificans*, the contributions of protonated and ionized carboxylic groups of the heme propionates were assigned by specific ^{13}C-labeling of the carboxylic groups of the four heme propionates (*36*). Comparison of the electrochemically induced FTIR difference spectra of wild-type and specific ^{13}C-labeled cytochrome *c* oxidase allowed assignment of a signal at 1676 cm^{-1} to contributions of protonated carboxylic groups. Difference bands at 1570 and 1538 cm^{-1} were assigned to the $\nu(COO^-)^{as}$ vibration and at 1380 cm^{-1} to the $\nu(COO^-)^{s}$ vibration of deprotonated heme propionates. The analysis of the difference spectra strongly suggests that the heme propionates in the cytochrome *c* oxidase from *P. denitrificans* are partially protonated (*36*). The difference signals in the characteristic spectral range for the ν(C═O) mode of protonated carboxylic groups of the heme propionates are significantly stronger in the electrochemically induced FTIR difference spectra of the ba_3 oxidase from *T. thermophilus* than for the aa_3 oxidase in *P. denitrificans*. The signals are composed of a negative signal at 1672 cm^{-1} (Figure 3b) and a positive signal at 1676 cm^{-1}, where the contributions of the protonated heme propionates and of the formyl group can be expected. Furthermore, the contributions in the typical spectral range of the ionized form are significantly weaker. Differences in protonation state and environment of the carboxylic groups in the cytochrome *c* oxidase from *P. denitrificans* and *T. thermophilus* are probable, and the spectra presented here indicate that the propionates in the ba_3 oxidase from *T. thermophilus* are essentially protonated.

Assignment of Polypeptide Backbone Modes. Amide I signals are predominantly caused by the C═O stretching vibrations of the polypeptide backbone with frequencies characteristic for specific secondary structure elements. In the electrochemically induced FTIR difference spectra, contributions from the reorganizations of the polypeptide backbone upon reduction/oxidation of the cofactors can be expected, and the partial attribution of the signals to amide I modes is conceivable. In the amide I region (1690−1610 cm^{-1}), strong negative difference signals can be observed at 1630 and 1668 cm^{-1} with a shoulder at 1662 cm^{-1} (Figure 3a). Positive signals can be seen at 1678, 1656, and 1646 cm^{-1}. H/D exchange (Figure 3b) causes the decrease of the difference signals at 1678 and 1656 cm^{-1} and the increase of the signals at 1668 and 1646 cm^{-1}. The difference signals at 1662 and 1656 cm^{-1} absorb in the spectral range characteristic for α-helical secondary structure elements. These signals show very small changes upon H/D exchange, as expected for α-helical secondary structure elements (2−10 cm^{-1}) (*59*), thus supporting the tentative assignment to α-helical secondary structure elements.

The difference signals observed at 1646 and 1630 cm^{-1} absorb in a spectral range characteristic for β-sheet secondary structure elements. For the difference signals at 1678 and 1668 cm^{-1}, the involvement of β-sheet secondary structure elements should be considered, too. However, conclusive assignments are difficult here. Further groups are probably involved in the difference signals discussed for the amide I region (cf. Table 1).

Amide II modes result mainly from coupled C−N stretching and N−H bending vibrations. H/D exchange induces the

Table 1: Assignments for the Electrochemically Induced FTIR Difference Spectra Presented in Figures 2 and 4

position of H_2O in spectrum (cm^{-1})	position of D_2O in spectrum (cm^{-1})	redox state	tentative assignments
1738	1732		ν(C═O) Asp/Glu
1708	1706	ox	ν(C═O) heme propionates
1698		red	ν(C═O) heme propionates
1692	1692	ox	ν(C═O) heme propionates
1688	1686	red	amide I (β-sheet)
1678	1676	ox	ν(C═O) CHO-heme a_3
			ν(C═O) heme propionates
			$\nu(CN_3H_5)^{as}$ Arg
			Asn,Gln
1668	1668	red	ν(C═O) CHO-heme a_3
1664	1662	red	amide I (α-helical)
1656	1654	ox	amide I (α-helical)
1646	1646	ox	amide I (α-helical)
1630	1630	red	$\nu(CN_3H_5)^{s}$Arg
			Lys, His-H
			amide I (β-sheet)
1618	1618	red	ν(Cα=Cβ) vinyl group (heme b/a_3)
			amide I (β-sheet)
1610		ox	ν_{37} heme a_3
1590		ox	Ring-O^- Tyr
			His
1570	1570	ox	$\nu(COO^-)^{as}$ heme propionates
			Ring-O^- Tyr
			ν_{37} heme b
			ν_{38x} heme a_3
1554	1554	red	ν_{37} heme b
1542	1542	red	ν_{38y} heme a_3
1536	?	ox	?
1528		ox	$\nu(COO^-)^{as}$ heme propionates?
1518	1518	red	Ring-OH Tyr
1504	1504	ox	Ring-O^- Tyr
1434		ox	$\nu(COO^-)^{s}$ Asp/Glu
1418	1418	red	$\nu(COO^-)^{s}$ Asp/Glu
1404		ox	?
1390		red	$\nu(COO^-)^{s}$ heme propionates
1380			ν_{41} heme a/a_3
1280	1280	red	$\nu(CO^-)^{s}$ Tyr
1266	1262	ox	δ_{42} heme b/a_3
1160	1182		P═O
1088			P═O

uncoupling of the C−N and the N−H vibration and shifts the N−D bending mode to 1490−1460 cm^{-1} and the C−N stretching mode to wavenumbers below 1100 cm^{-1}. In the amide II region from 1575 to 1480 cm^{-1}, several overlapping difference signals can be observed. An assignment of these difference signals to amide II modes appears less probable since little or no shift of these signals upon H/D exchange can be reported (see Figure 4a−c).

Assignment of Individual Amino Acid Side Chain Modes. (A) Aspartic and Glutamic Acid Side Chain Modes. The ν(C═O) mode of protonated aspartic and glutamic acid side chains can be expected at wavenumbers above approximately 1710 cm^{-1}, at positions depending on the hydrogen bonding to/from the COOH group. In this spectral region, no significant difference signals can be observed revealing that no protonated aspartic and glutamic acid is contributing in the electrochemically induced FTIR difference spectra of the ba_3 oxidase from *T. thermophilus*.

In the electrochemically induced FTIR difference spectra of wild-type cytochrome *c* oxidase from *P. denitrificans*, mutants in the discussed proton pathways (Glu-278 and Asp-124) clearly allowed assignment of Glu-278 to a difference signal at 1746/1734 cm^{-1} (*35*). Puustinen et al. (*32*), using a different approach (light-induced difference spectra of CO-poisoned oxidase at 80 K), discuss the involvement of the corresponding amino acid Glu-286 in the bo_3 oxidase from *E. coli* to a difference signal with a comparable absorption. Glutamic acid 278 (numbering for *P. denitrificans* oxidase) is discussed to play a crucial role in the catalytic cycle of cytochrome oxidase, and aspartic acid 124 is discussed to be the first proton acceptor in the D-pathway. In the ba_3 oxidase from *T. thermophilus*, however, Glu-278 and Asp-124 are not conserved and are replaced by uncharged residues (Asn and Ile). This significantly deviates from the majority of known oxidases where these groups are conserved.

The $\nu(COO^-)^{as}$ mode of ionized aspartic and glutamic acid side chains absorbs between 1580 and 1560 cm^{-1} and the corresponding $\nu(COO^-)^{s}$ mode at approximately 1400−1420 cm^{-1} based on investigations of isolated amino acids (*60*). In the respective spectral range in the electrochemically induced FTIR difference spectra, signals can be observed at 1570, 1434, 1418, and 1402 cm^{-1} (Figure 3a−c). A possible assignment of the difference signals to $\nu(COO^-)^{as}$ modes should be in line with the strong increase of signal intensity of the $\nu(COO^-)^{as}$ mode upon H/D exchange in model compounds. In the electrochemically induced FTIR difference spectra in D_2O (Figure 4a−c), no increase of the difference signals around 1570 cm^{-1} can be reported as compared to H_2O (Figure 4a−c), suggesting that no ionized aspartic and glutamic acid side chains contribute in the electrochemically induced FTIR difference spectra. We note that the discussed spectral region is very complex and several difference signals overlap here; conclusive assignments can only be made on the basis of labeling experiments on aspartic and glutamic acid side chains in the protein.

(B) Tyrosine. The ring vibration of protonated tyrosine side chains absorbs at approximately 1516 cm^{-1} and in the ionized form at 1560 and 1498 cm^{-1} with relatively strong absorptions (*60*). Another characteristic absorption for ionized tyrosine groups can be expected at approximately 1269 cm^{-1} (*60*). In the electrochemically induced FTIR difference spectra shown in Figure 3a,b a negative difference band at 1516 cm^{-1} and in Figure 3a−c positive difference bands at 1504, 1570, and 1262 cm^{-1} are observed. A possible interpretation for the observed difference bands is the deprotonation/protonation of a tyrosine group coupled to electron transfer from/to heme *b* (Figure 3b) or the change of environment of a deprotonated tyrosine group coupled to heme a_3 (Figure 3c). The additional involvement of other signals in this spectral range, for example, heme modes, has to be considered.

A critical tyrosine group would be Tyr-237 (numbering for the ba_3 oxidase from *T. thermophilus*), a group close to the binuclear center, that is conserved in other oxidases (*4*, *7*). The structures of cytochrome *c* oxidase from *P. denitrificans* and from bovine heart oxidase indicate that Tyr-280 (numbering for *P. denitrificans*) is covalentely linked to His-276 (*4*; for bovine heart oxidase, see *7*). This cross-link could be chemically evidenced for the ba_3 oxidase from *T. thermophilus* (*8*). Thus, similar contributions in the IR spectra of the cytochrome *c* oxidase from *P. denitrificans* and *T. thermophilus* are conceivable. This uncommon structure

might exhibit uncommon absorptions in the IR due to the reduced symmetry of the ring and may provide a possible explanation for the relatively weak intensity of the signal at 1516 cm^{-1}, in comparison to the signal intensity of isolated tyrosines (*60*).

(C) Arginine. Arginine side chains show IR modes at approximately 1673 cm^{-1} [$\nu(CN_3H_5)^{as}$] and 1632 cm^{-1} [$\nu(CN_3H_5)^{s}$], as expected from studies on isolated arginines (*60*). Difference bands are observed in the spectra presented here at 1678 and 1630 cm^{-1}. Arginine side chains can be found in the vicinity of the active centers. However, the involvement of the contributions of other groups in these bands can be expected (see Table 1), and an alternative assignment to arginine side chains cannot be made without further investigations on mutants.

(D) Lysine. IR spectroscopic investigations on isolated amino acids revealed that lysines contribute at approximately 1629 cm^{-1} with a relatively small extinction coefficient (*60*). In the electrochemically induced FTIR difference spectra (Figure 4a,b) a strong negative signal can be seen at 1630 cm^{-1}. However, the assignment of this signal to β-sheet secondary structure elements and to the $\nu(CN_3H_5)^{s}$ mode from arginine side chains (discussed above) is more probable as judged from its intensity. In addition, spectra of other oxidases which contain heme *b* indicate that this signal might be a characteristic heme *b* mode (P. Hellwig unpublished results). The correlation of the signal at 1630 cm^{-1} with the heme *b* redox transition (Figure 3a) reinforces this possibility.

CONCLUSIONS

The electrochemical titrations of the ba_3 oxidase from *T. thermophilus* in the UV/VIS revealed two potentials for each heme with uncommon values and relative contributions. A comparison of these titrations to previously reported data from bovine heart cytochrome *c* oxidase (*46*−*51*) reveals a different cooperativity of the hemes and of Cu_B. A possible explanation for these deviations are differences in the environment of the active centers which cause different local electrostatics and thus can shift redox potentials and/or influence cooperativity. On the basis of the uncommon electrochemical properties, unique values for electron transfer and turnover as well as uncommon ligand binding dynamics can be expected and have already been partially reported (*25*).

The electrochemically induced FTIR difference spectra of the ba_3 oxidase heme modes, for example, the $\nu_{38x/y}$ mode of heme a_3, reveal uncommon absorbance maxima and thus indicate deviations at the porphyrin ring and/or its local site as compared to the cytochrome *c* oxidase from *P. denitrificans*. On the basis of the absorption of the heme a_3 formyl substituent [ν(C═O)], however, similarities in the direct environment of the formyl group can be expected. Absorptions characteristic for protonated heme propionates could be observed in the electrochemically induced FTIR difference spectra. They indicate that the heme propionates of hemes *b* and a_3 are predominantly protonated, deviating in their protonation state from the propionates in the cytochrome *c* oxidase from *P. denitrificans* (*36*). Some of the differences between the electrochemically induced FTIR difference spectra of the cytochrome *c* oxidase from *P. denitrificans* (*35*, *55*) and from *T. thermophilus* can be related to relevant amino acids which are not conserved in the ba_3 oxidase from *T. thermophilus* (Glu-278, Asp-124, Arg-54, and Lys-354).

The characterization of the electrochemical, UV/VIS, and FTIR spectroscopic properties of the ba_3 oxidase from *T. thermophilus* shows clear differences with respect to a large number of known oxidases and confirms previous observations made in resonance Raman spectra (*27*). The low sequence identity to most known oxidases, as well as amino acids which are not conserved and are discussed to be crucial in the catalytic cycle, offers a basis for the deviations. The unique properties of the aberrant ba_3 oxidase from *T. thermophilus* may reflect the phylogenetically ancient adaptation of the organism to extreme environmental conditions such as high temperature and low oxygen concentration and a convergent evolution of energy-conserving mechanisms (*30*).

ACKNOWLEDGMENT

We thank Christine Ernd for excellent technical assistance, Peter Hildebrandt (MPI für Strahlenchemie, Mühlheim) for critical reading of the manuscript, and Aimo Kannt (MPI für Biophysik, Frankfurt/M.) for discussions.

REFERENCES

1. Ferguson-Miller, S., and Babcock, G. T. (1996) *Chem. Rev.* 96, 2889−2907.
2. Michel, H., Behr, J., Harrenga, A., and Kannt, A. (1998) *Annu. Rev. Biophys. Biomol. Struct.* 27, 329−356.
3. Iwata, S., Ostermeier, C., Ludwig, B., & Michel, H. (1995) *Nature* 376, 660−669.
4. Ostermeier, C., Harrenga, A., Ermler, U., and Michel, H. (1997) *Proc. Natl. Acad. Sci. U.S.A. 94*, 10547−10553.
5. Tsukihara, T., Aoyama, H., Yamashita, E., Tomizaki, T., Yamaguchi, H., Shinzawa-Itoh, K., Nakashima, R., Yaono, R., and Yoshikawa, S. (1995) *Science 269*, 1069−1074.
6. Tsukihara, T., Aoyama, H., Yamashita, E., Tomizaki, T., Yamaguchi, H., Shinzawa-Itoh, K., Nakashima, R., Yaono, R., and Yoshikawa, S. (1996) *Science* 272, 1136−1144.
7. Yoshikawa, S., Shinzawa-Itoh, K., Nakashima, R., Yaono, R., Yamashita, E., Inoue, N., Yao, M., Fei, M. J., Libeu, C. P., Mizushima, T., Yamaguchi, H., Tomizaki, T., and Tsukihara, T. (1998) *Science* 280, 1723−1729.
8. Buse, G., Soulimane, T., Dewor, M., Meyer, H. E., and Blüggel, M. (1999) *Protein Sci.* (in press).
9. Hosler, J. P., Shapleigh, J. P., Mitchell, D. M., Kim, Y., Pressler, M. A., Georgiou, C., Babcock, G. T., Alben, J. O., Ferguson-Miller, S., and Gennis, R. B. (1996) *Biochemistry* 35, 10776−10783.
10. Ädelroth, P., Gennis, R. B., and Brzezinski, P. (1998) *Biochemistry* 37, 2470−2476.
11. Pfitzner, U., Odenwald, A., Ostermann, T., Weingard, L., Ludwig, B., and Richter, O.-M. H. (1998) *J. Bioenerg. Biomembr. 30*, 89−97.
12. Vygodina, T. V., Pecorano, C., Mitchell, D., Gennis, R., and Konstantinov, A. A. (1998) *Biochemistry 37*, 3053−3061.
13. Zaslavsky, D., and Gennis, R. (1998) *Biochemistry 37*, 3062−3067.
14. Ädelroth, P., Svensson-Ek, M., Mitchell, D. M., Gennis, R. B., & Brzezinski, P. (1997) *Biochemistry 36*, 13824−13829.
15. Konstantinov, A. A., Siletsky, S., Mitchell, D., Kaulen, A., & Gennis, R. B. (1997) *Proc. Natl. Acad. Sci. U.S.A. 94*, 9085−9090.
16. Fee, J. A., Choc, M. G., Findling, K. L., Lorence, R., & Yoshida, T. (1980) *Proc. Natl. Acad. Sci. U.S.A. 77*, 147−151.
17. Zimmermann, B. H., Nitsche, C. I., Fee, J. A., Rusnak, F., & Munck, E. (1988) *Proc. Natl. Acad. Sci. 85*, 5779−5783.
18. Lübben, M., & Morand, K. (1994) *J. Biol. Chem. 269*, 21473−21479.

19. Bresser, A. H., & Buse, G. (1993) *Biol. Chem. Hoppe-Seyler 374*, 736.
20. Keightley, J. A., Zimmermann, B. H., Mather, M. W., Springer, P., Pastuszyn, A., Lawrence, D. M., and Fee, J. A. (1995) *J. Biol. Chem*. 270, 20345−20358.
21. Giuffrè, A., Forte, E., Antonini, G., D'Itri, E., Brunori, M., Soulimane, T., and Buse, G. (1999) *Biochemistry 38*, 1057−1065.
22. Soulimane, T., von Walter, M., Hof, P., Than, M. E., Huber, R., & Buse, G. (1997) *Biochem. Biophys. Res. Commun. 237*, 572−576.
23. Castresana, J., and Saraste, M. (1995) *Trends Biochem. Sci*. 20, 443−448.
24. Schäfer, G., Purschke, W., and Schmidt, C. L. (1996) *FEMS Microbiol. Rev. 18*, 173−188.
25. Einarsdottir, O., Killough, P. M., Fee, J. A., and Woodruff, W. H. (1989) *J. Biol. Chem. 264*, 2405−2408.
26. Surerus, K. K., Oertling, W. A., Fan, C., Gurbiel, R. J., Einarsdottir, O., Antholine, W. E., Dyer, R. B., Hoffman, B. M., Woodruff, W. H., and Fee, J. A. (1992) *Proc. Natl. Acad. Sci. U.S.A. 89*, 3195−3199.
27. Oertling, W. A., Surerus, K. K., Einarsdottir, O., Fee, J. A., Dyer, R. B., and Woodruff, W. H. (1994) *Biochemistry 33*, 3128−3141.
28. Goldbeck, R. A., Einarsdottir, O., Dawes, T. D., O'Connor, D. B., Surerus, K. K., Fee, J. A., and Kliger, S. S. (1992) *Biochemistry 31*, 9376−9387.
29. Soulimane, T., Gohlke, U., Huber, R., and Buse, G. (1995) *FEBS Lett. 368*, 132−134.
30. Kannt, A., Soulimane, T., Buse, G., Becker, A., Bamberg, E., and Michel, H. (1998) *FEBS Lett. 434*, 17−22.
31. Park, S., Pan, L. P., Chan, S. I., and Alben, J. O. (1996) *Biophys. J. 71*, 1036−1047.
32. Puustinen, A., Bailey, J. A., Dyer, R. B., Mecklenburg, S. L., Wikström, M., and Woodruff, W. H. (1997) *Biochemistry 36*, 13195−13200.
33. Lübben, M., and Gerwert, K. (1996) *FEBS Lett. 397*, 303−307.
34. Hellwig, P., Rost, B., Kaiser, U., Ostermeier, C., Michel, H., and Mäntele, W. (1996) *FEBS Lett. 385*, 53−57.
35. Hellwig, P., Behr, J., Ostermeier, C., Richter, O.-M. H., Pfitzner, U., Odenwald, A., Ludwig, B., Michel, H., and Mäntele, W (1998) *Biochemistry 37*, 7390−7399.
36. Behr, J., Hellwig, P., Mäntele, W., and Michel, H. (1998) *Biochemistry 37*, 7400−7406.
37. Moss, D. A., Nabedryk, E., Breton, J., and Mäntele, W. (1990) *Eur. J. Biochem. 187*, 565−572.
38. Mäntele, W. (1996) in *Biophysical Techniques in Photosynthesis* (Hoff, A. J., and Amesz, J., Eds.) Chapter 9, pp 137−160, Kluwer, Dordrecht.
39. Mäntele, W. (1993) *Trends Biochem. Sci*. 18, 197−202.
40. Wikström, M., and Morgan, J. E. (1992) *J. Biol. Chem. 267*(15), 10266−10273.
41. Morgan, J. E., Verkhovsky, M. I., and Wikström, M. (1996) *Biochemistry 35*, 12235−12240.
42. Babcock, G. T. (1988) in *Raman Scattering by Cytochrome Oxidase and by Heme a Model Compounds*. Chapter 7 of *Biological Applications of Resonance Raman Spectroscopy* (Spiro, T., Ed.) Wiley and Sons, New York.
43. Mitchell, R., Mitchell, P., and Rich, P. R. (1991) *FEBS Lett. 280*, 321−324.
44. Lappalainen, P., Aasa, R., Malmström, B. G., and Saraste, M. (1993) *J. Biol. Chem. 35*, 26416−26421.
45. Lappalainen, P., Waltmough, N. J., Greenwood, C., and Saraste, M. (1995) *Biochemistry 34*, 5824−5830.
46. Nicholls, P., and Petersen, L. C. (1972) *Biochim. Biophys. Acta 357*, 462−467.
47. Wikström, M. K., Krab, K., and Saraste, M. (1981) *Cytochrome oxidase, A synthesis*, 198 pp, Academic Press, New York.
48. Wikström, M. K. F., Harmon, H. J., Ingledew, W. J., and Chance, B. (1976) *FEBS Lett. 65*(3) 259−277.
49. Hendler, R. W., and Westerhoff, H. V. (1992) *Biophys. J. 63*, 1586−1604.
50. Carter, K., and Palmer, G. (1982) *J. Biol. Chem*. *257*(2), 13507−13514.
51. Babcock, G. T., Vickery, L. E., and Palmer, G. (1978) *J. Biol. Chem. 7*, 2400−2411.
52. Heibel, G. E., Hildebrandt, P., Ludwig, B., Steinrücke, P., Soulimane, T., and Buse, B. (1993) *Biochemistry 32*, 10866−10877.
53. Gerscher, S., Hildebrandt, P., Soulimane, T., and Buse, G. (1998) *Biospectroscopy 4*(6), 365−377.
54. Spiro, T. G., and Li, X.-Y (1988) *Resonance Raman Spectroscopy of Metalloporphyrins.* Chapter 1 in *Biological Applications of Resonance Raman Spectroscopy*, Wiley and Sons, New York.
55. Hellwig, P., Grzybek, S., Behr, J., Ludwig, B., Michel, H., and Mäntele, W. (1999) *Biochemistry 38*, 1685−1694.
56. Li, X.-Y., Czernuszewicz, R. S., Kincaid, J. R., Su, Y. O., and Spiro, T. G. (1990) *J. Phys. Chem. 94*, 31−47.
57. Berthomieu, C., Boussac, A., Mäntele, W., Breton, J., and Nabedryk, E. (1992) *Biochemistry 31*, 11460−11471.
58. Gerscher, S. (1997) Ph.D. Thesis, Heinrich Heine Universität, Düsseldorf.
59. Arrondo, J. L. R., Muga, A., Castresana, J., and Goni, F. M. (1993) *Prog. Biophys. Mol. Biol. 59*, 23−56.
60. Venyaminov, S. Y., and Kalnin, N. N. (1990) *Biopolymers* 30, 1259−1271.

BI9903401